Appl. Phys. A (2014) 116:703–713
DOI 10.1007/s00339-014-8505-1

Applied Physics A
Materials Science & Processing

Modulation of diffusion with polarized lasers

Sen-Yong Chen · Othmane Benafan · Raj Vaidyanathan · Aravinda Kar

Received: 30 September 2013 / Accepted: 12 May 2014 / Published online: 14 June 2014

Abstract Laser diffusion is generally used to modify the metallurgical composition at the surface of materials for improving the mechanical properties. Platinum has been diffused into titanium and tantalum sheets in this study, and the concentrations of Pt in the substrates are determined. The concentration of Pt is higher at lower scanning speeds due to higher surface temperature and longer diffusion time than in the case of higher scanning speeds. Additionally, the samples treated with a linearly polarized laser beam exhibit slightly higher concentration of Pt. The enhanced diffusion in the case of linearly polarized laser treatment can be attributed to controlled excitation of the local vibration modes of the atoms in the substrate. The reflectivity of the samples are also measured at the wavelength of 1,064 nm and compared with theoretical results.

S.-Y. Chen · A. Kar (✉)
Laser-Advanced Materials Processing Laboratory, CREOL, The College of Optics and Photonics, University of Central Florida, 4000 Central Florida Blvd, Orlando, FL 32816, USA
e-mail: akar@creol.ucf.edu

O. Benafan · R. Vaidyanathan
Advanced Materials Processing and Analysis Center (AMPAC), Mechanical, Materials, and Aerospace Engineering, University of Central Florida, 4000 Central Florida Blvd, Orlando, FL 32816, USA
e-mail: othmane.benafan@nasa.gov

R. Vaidyanathan
e-mail: raj@ucf.edu

Present Address:
O. Benafan
Structures and Materials Division, NASA Glenn Research Center, Cleveland, OH 44135, USA

1 Introduction

Lasers have become important tools for a wide range of materials processing applications. Traditionally laser diffusion has been implemented to improve the mechanical properties of materials, such as hardness and wear resistance, by altering the metallurgical composition at the surface of materials. This technique has also been used to fabricate semiconductor devices such as light-emitting diodes [1], chemical sensors [2] and transistors [3]. Highly directional and rapid energy delivery capability of lasers, and controlled temperature distribution and thermal depth in the substrate are some of the unique characteristics that make laser diffusion an attractive process. The heating and cooling rates and the temperature distribution can be controlled by various processing parameters such as the laser irradiance, laser–substrate interaction time, laser scanning speed and the ambience surrounding the substrate. The temperature of the substrate can be rapidly raised to very close to its melting temperature without affecting the material around the heating zone. In this non-isothermal, localized high temperature region, the impurity diffusion coefficient increases significantly, enhancing the migration of diffusants. Another attractive feature of laser diffusion is that it is a maskless process because the diffusant atoms can be incorporated into selective regions without any photolithography steps.

The motion of the diffusant atoms can be restricted to certain directions by utilizing the polarization of lasers. Polarization, which is the direction of the electric field amplitude vector of the laser at a spatial point over one period of oscillation, is generally perpendicular to the direction of the laser propagation. The oscillation direction of the electric field can be confined to a straight line (linear polarization) or rotated (circular polarization) as the laser

beam propagates. The effects of polarizations have been analyzed by Petring et al. [4], and Niziev and Nesterov [5] for laser cutting and by Ho [6] for a special case of laser welding and drilling. Artsimovich et al. [7] showed that the diffusion coefficient of oxygen atoms in silicon substrates increases when the substrate is irradiated with a laser beam of polarization parallel to the Si–O–Si bonds. Pavlovich [8] explained theoretically that the diffusion coefficient of oxygen is enhanced when the photon energy is comparable to the vibrational energy of the silicon lattice and the polarization direction is parallel to the direction of anti-symmetric vibration of oxygen atoms along <111>. Increased concentration gradient of oxygen along <111> also enhances its diffusion.

Besides the photon energy and polarization, the laser irradiance profile affects the migration of diffusants significantly through thermal energy distribution in the material, resulting in highly energetic phonons. Laser resonators generally produce laser beams of Gaussian irradiance profiles. However, spatially uniform irradiance profiles allow more uniform surface heating than Gaussian beams, resulting in planes of constant diffusant concentration at various depths of the substrate. Numerous techniques have been studied to transform Gaussian laser beams into flat-top beams of uniform irradiance profile. The flat-top beam can be produced by absorptive [9], refractive [10], reflective [11] and diffractive [12] optical elements. Due to the poor optical conversion efficiency of the absorptive elements, they are unsuitable for high-power lasers. Refractive, reflective and diffractive optical elements can have high optical conversion efficiency. A beam shaping lens is designed in this study for producing a uniform irradiance profile from a Gaussian beam. The vector diffraction theory is used in this study to design a beam shaping lens by considering the diffraction effect and the longitudinal component of the laser polarization for producing a uniform irradiance profile from a Gaussian beam.

The focus of this paper is threefold: (1) Modify the surface chemistry of selected biomaterials by diffusing a trace amount of another material such as Pt. (2) Measure the reflectivity of selected biomaterials for different polarizations of a Nd:YAG laser of wavelength 1,064 nm. This datum is important because absorptivity, which is related to the reflectivity, affects the temperature of the material during laser heating and thus influences the diffusion process. (3) Examine the effect of laser polarization on the diffusion of Pt, since polarized lasers can govern the vibrations of atoms, i.e., phonons, in a certain direction and thus affect the diffusion mechanism for the migration of atoms. These three objectives are accomplished by employing three conventional methods, a laser-assisted diffusion process, a reflectivity measurement technique and laser beam shaping, to incorporate Pt into selected biomaterials.

Although the laser beam shaping is well known, the utilization of laser polarization provides a novel mechanism to influence the diffusion process by confining the atomic migration in a certain direction. Laser-assisted diffusion into a substrate, which is a non-equilibrium process, has been shown to incorporate excess diffusant atoms exceeding the solid solubility limit of the substrate [13, 14]. The effect of polarization on the diffusion of Pt, which was not studied in [13, 14] has been examined in this paper.

Thin sheets of Ti and Ta have been chosen as substrates to diffuse Pt into them using a laser-assisted diffusion process. These three elements are biocompatible materials [15, 16] with numerous medical applications such as plates, rods and screws in different orthopedic treatments for joining bones. Although Pt, Pd and Au are excellent biomaterials due to their chemical stability and high corrosion resistance in biofluids, they are too expensive to have an entire implant made of these materials. Ti and its alloys are often preferred; however, certain implants of these materials are found to fail in clinical tests in spite of their satisfactory performance in in vitro conditions [15]. Since a coating of Pt on Ti can induce galvanic corrosion, an approach to modify the surface chemistry would be diffusing Pt into the substrate.

2 Theoretical analysis

2.1 Beam shaping lens design

A beam shaping lens is shown in Fig. 1 for transforming a Gaussian beam into a flat-top beam. The incident Gaussian beam has a radius w' and the flat-top beam has a radius w. The thickness of the lens at its center is t_c. The distance between the back surface of the lens and the target plane is D. The design of the beam shaping lens is based on vector diffraction theory which accounts for the polarization of the laser.

If a region is free of electrical charges and the field at the aperture plane S' is $\vec{U}'\left(\vec{r}'\right)$, the diffracted field at any radial vector $\vec{r}$ and distance is given by [17, 18]:

$$\vec{U}\left(\vec{r}\right) = \frac{1}{2\pi}\nabla \times \iint_{S'} \hat{z} \times U'\left(\vec{r}\prime\right) \frac{\exp(-i\beta\rho)}{\rho} \mathrm{d}a' \qquad (1)$$

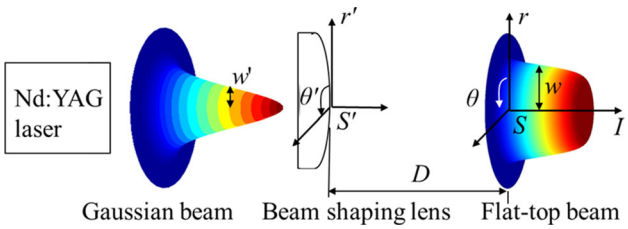

Fig. 1 A beam shaping lens that transforms a Gaussian beam into a flat-top beam

where β is the wave number which is equal to $2\pi/\lambda_L$, λ_L is the wavelength of the laser, $\hat{z}$ is the unit vector in the direction of laser beam propagation and da' is the differential area on the aperture plane. ρ is the distance from a point on the lens to a point on the target plane S and can be written as:

$$\rho = \left|\vec{r} - \vec{r}'\right| = \sqrt{(x-x')^2+(y-y')^2+(z-z')^2} \tag{2}$$

where (x', y', z') and (x, y, z) are the Cartesian coordinates of points on the aperture and target planes, respectively. Substituting Eq. (2) into Eq. (1), one can express the three components of $\vec{U}(\vec{r})$ as:

$$U_j(x,y,z) = \frac{i\beta z}{2\pi}\iint_{S'} U_{j'}(x\prime,y\prime,0) \times \left(1+\frac{1}{i\beta\rho}\right)\frac{\exp(-i\beta\rho)}{\rho^2}\mathrm{d}x'\mathrm{d}y', \quad j = x \text{ and } y \tag{3}$$

$$\begin{aligned} U_z(x,y,z) = &-\frac{i\beta}{2\pi}\iint_{S'}\left[U'_x\left(x',y',0\right)\left(x-x'\right)\right. \\ &\left.+U'_y\left(x',y',0\right)\left(y-y'\right)\right] \\ &\times\left(1+\frac{1}{i\beta\rho}\right)\frac{\exp(-i\beta\rho)}{\rho^2}\mathrm{d}x'\mathrm{d}y' \\ &+\frac{1}{2\pi}\iint_{S'}\left[\frac{\partial U'_x(x',y',0)}{\partial x'}+\frac{\partial U'_y(x',y',0)}{\partial y'}\right] \\ &\times\frac{\exp(-i\beta\rho)}{\rho}\mathrm{d}x'\mathrm{d}y' \end{aligned} \tag{4}$$

Assuming $\rho >> \lambda_L$, $z >> x - x'$ and $z >> y - y'$, one can express Eqs. (3) and (4) as:

$$U_j(x,y,z) = \frac{i\beta}{2\pi z}\iint_{S'} U'_j(x',y',0)\Phi_{xy}\mathrm{d}x'\mathrm{d}y', \quad j = x \text{ and } y \tag{5}$$

$$\begin{aligned} U_z(x,y,z) = &-\frac{i\beta}{2\pi z^2}\iint_{S'}\left[U'_x(x',y',0)(x-x')+U'_y(x',y',0)\right. \\ &\left.\times(y-y')\right]\Phi_{xy}\mathrm{d}x'\mathrm{d}y' \\ &+\frac{i\beta}{2\pi z}\iint_{S'}\left[\frac{\partial U'_x(x',y',0)}{\partial x'}+\frac{\partial U'_y(x',y',0)}{\partial y'}\right] \\ &\Phi_{xy}\mathrm{d}x'\mathrm{d}y' \end{aligned} \tag{6}$$

where Φ_{xy} is defined as:

$$\Phi_{xy} = \exp\left\{-i\frac{\beta z}{2}\left[1+\frac{(x-x')^2+(y-y')^2}{z^2}\right]\right\} \tag{7}$$

Equation (5) is identical to the Fresnel diffraction equation derived from the scalar diffraction theory. The longitudinal component, which is given by Eq. (6), does not appear in the scalar diffraction theory.

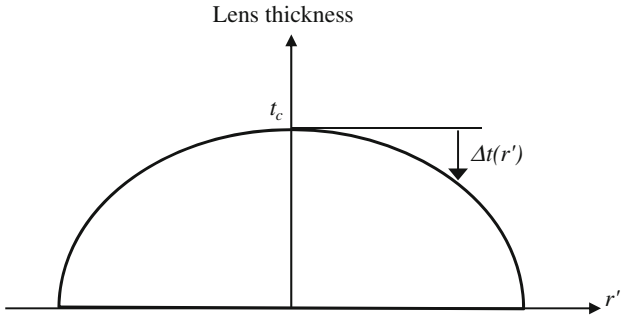

Fig. 2 Geometrical features of the beam shaping lens, showing the thickness (t_c) and surface sag ($\Delta t(r')$) as a function of the radius (r') of the lens

Assuming that the incident beam has a Gaussian irradiance profile and that the beam shaping lens modifies only the phase, the electric field at the back surface of the lens can be expressed as:

$$U'_j(x',y',0) = U'_{j0}(x',y',0)\exp\left(-\frac{x'^2+y'^2}{w'^2}+i\phi'(x',y')\right), \quad j = x \text{ and } y \tag{8}$$

where U'_{j0} is the amplitude of the electric field of the incident laser beam and $\phi'(x',y')$ is the optical phase contributed by the beam shaping lens. $\phi'(x',y')$ can be expressed as follows in terms of refractive index n, center thickness t_c and surface sag $\Delta t(x',y')$ of the beam shaping lens as shown in Fig. 2.

$$\phi'(x',y') = \beta t_c - \beta(n-1)\cdot\Delta t(x',y') \tag{9}$$

The laser irradiance on the target plane is given by:

$$I(x,y,z) = \sum_j \left|U_j(x,y,z)\right|^2, \quad j = x,y \text{ and } z \tag{10}$$

Equations (5), (9) and (10) show that the laser irradiance on the target plane depends on the optical phase altered by the thickness of the beam shaping lens. So a flat-top beam can be obtained by designing the surface sag, $\Delta t(x',y')$, of the beam shaping lens.

In this study, the design of the beam shaping lens is based on fused silica of refractive index 1.45 at the wavelength of 1,064 nm. Other relevant parameters for the design are $w' = 0.5$ mm, $w = 5.5$ mm, $t_c = 8$ mm, $D = 80$ mm and the lens diameter $D_l = 25.4$ mm. Plano-convex lenses are considered in this study since they are fabricated more easily than plano-concave lenses. The surface sag of the lens is found to be:

$$\Delta t\left(x',y'\right) = -\frac{0.248\times\left(x'^2+y'^2\right)}{1+\sqrt{1+(1-19)\times0.248\times(x'^2+y'^2)}} \tag{11}$$

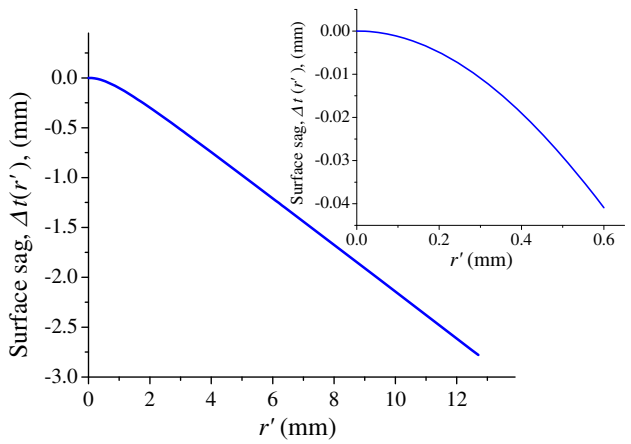

Fig. 3 Surface sag of the beam shaping lens. The *inset* shows the surface sag at the central portion of the beam shaping lens

which can be readily rewritten in cylindrical coordinates by noting that $r'^2 = x'^2 + y'^2$.

The surface sag is plotted in Fig. 3, showing how the thickness varies with the radius of the beam shaping lens. The radius of the laser beam is 0.5 mm in this study, and it is incident at the central region of the lens. The lens has a curved shape near the central region as shown in the inset in Fig. 3. The shape of the lens varies almost linearly for $r' > 2$ mm.

2.2 Rough surface reflection model: effect of polarization on the reflectivity of rough surfaces

The reflectivity of isotropic, homogeneous materials with perfectly smooth surface can be determined from the Fresnel equations [19]:

$$R_{\mathrm{Fp}} = \frac{(n^2 - n\cos\theta_t)^2 + (2n^2\kappa - \kappa\cos\theta_t)^2}{(n^2 + n\cos\theta_t)^2 + (2n^2\kappa + \kappa\cos\theta_t)^2} \tag{12}$$

$$R_{\mathrm{Fs}} = \frac{(\cos\theta_i - n\cos\theta_t)^2 + \kappa\cos^2\theta_t}{(\cos\theta_i + n\cos\theta_t)^2 + \kappa\cos^2\theta_t} \tag{13}$$

where R_{Fp} and R_{Fs} are the Fresnel reflectivities for *p*-polarization and *s*-polarization, respectively, and θ_i and θ_t are the incident and refraction angles, respectively. n and κ are the refraction and absorption indices of the sample, respectively. θ_t is given by $\theta_t = \sin^{-1}\left(\frac{\sin\theta_i}{n+i\kappa}\right)$. Equations (12) and (13) show that the Fresnel reflectivities are the same for the *p*- and *s*-polarizations at the normal angle of incidence. However, the surface roughness and the anisotropic orientation of crystalline planes are expected to affect the reflectivity. A model [19], which considers the surface roughness, polarization and shadowing, is used in this study to calculate the theoretical reflectivity of samples irradiated by polarized laser beams. The surface properties can be described by an effective roughness, ρ_{eff}, in terms of the root-mean-square surface roughness, ρ_{rms}, as given by:

$$\rho_{\mathrm{eff}} = \rho_{\mathrm{rms}} \frac{1}{\sqrt{1 + \left(\frac{\zeta_0}{\rho_{\mathrm{rms}}}\right)^2}} \tag{14}$$

where ζ_0 is the root of the following equation:

$$\sqrt{\frac{\pi}{2}}\zeta_0 = \frac{\rho_{\mathrm{rms}}}{4}[K(\theta_i) + K(\theta_r)]\exp\left(-\frac{\zeta_0^2}{2\rho_{\mathrm{rms}}^2}\right) \tag{15}$$

with $\mathrm{K}(\theta) = \tan\theta \cdot \mathrm{erfc}\left(\frac{L_c}{2\rho_{\mathrm{rms}}}\cot\theta\right)$ and L_c as the coherence length of the surface asperity. θ_r is the reflected angles, respectively.

For rough surfaces, the reflectivity was studied [20–23] by considering a bidirectional reflectance distribution function (BRDF) $\bar{R}_b$, which is defined as the ratio of the reflected intensity (I_r) in a given direction to the incident energy per unit time (E_i) from another direction within a small solid angle, i.e., $\bar{R}_b = I_r/E_i$. Since the intensity represents the amount of energy per unit time per unit projected area per unit solid angle, the incident energy per unit time can be expressed in terms of the incident intensity (I_i) and the differential solid angle ($d\omega_i$) by the expression $E_i = I_i\cos\theta_i d\omega_i$ for an incident angle θ_i. $\bar{R}_b$ consists of two components:

$$\bar{R}_b(\theta_r, \rho_{\mathrm{rms}}) = \bar{R}_{\mathrm{bs}}(\theta_i, \rho_{\mathrm{rms}}) + \bar{R}_{bd}(\theta_r, \rho_{\mathrm{rms}}) \tag{16}$$

where $\bar{R}_{\mathrm{bs}}$ is the specular BRDF, $\bar{R}_{\mathrm{bd}}$ is the diffuse BRDF. It should be noted that $\theta_r \neq \theta_i$ for diffused reflection of the laser beam. The two components can be expressed as:

$$\bar{R}_{\mathrm{bs}} = \frac{R_{\mathrm{F}}F_{\mathrm{S}}(\theta_i)\exp(-F_\rho)}{\cos\theta_i d\omega_i} \tag{17}$$

$$\bar{R}_{\mathrm{bd}} = \frac{R_{\mathrm{F}}}{\pi}\frac{F_{\mathrm{G}}F_{\mathrm{D}}F_{\mathrm{S}}(\theta_i)F_{\mathrm{S}}(\theta_{\mathrm{r}})}{\cos\theta_i \cdot \cos\theta_{\mathrm{r}}} \tag{18}$$

where R_{F} is the Fresnel reflectivity which is given by Eqs. (12) and (13) for *p*- and *s*-polarizations, respectively. For other polarizations, such as random, circular and azimuthal polarizations, R_F is taken as the arithmetic average of R_{Fp} and R_{Fs}. $F_s(\theta)$ is the shadowing function, F_ρ is the surface roughness function, F_G is the geometrical function and F_D is the light distribution function, which are given by

$$F_{\mathrm{S}}(\theta) = \frac{1 - \frac{1}{2}\mathrm{erfc}\left(\frac{L_c\cot\theta}{2\rho_{\mathrm{rms}}}\right)}{1 + \frac{1}{2}\left[\frac{2}{\sqrt{\pi}}\frac{\rho_{\mathrm{rms}}}{L_c\cot\theta} - \mathrm{erfc}\left(\frac{L_c\cot\theta}{2\rho_{\mathrm{rms}}}\right)\right]} \tag{19}$$

$$F_\rho = \left[\frac{2\pi\rho_{\mathrm{eff}}}{\lambda_L}(\cos\theta_i + \cos\theta_r)\right]^2 \tag{20}$$

$$F_G = \left(\frac{\vec{k}_{\mathrm{d}} \cdot \vec{k}_{\mathrm{d}}}{k_{\mathrm{dz}}}\right)^2 \frac{1}{\left|\hat{k}_r \times \hat{k}_i\right|^4}\left[\left(\hat{s}_r \cdot \hat{k}_i\right)^2 + \left(\hat{p}_r \cdot \hat{k}_i\right)^2\right] \times \left[\left(\hat{s}_i \cdot \hat{k}_r\right)^2 + \left(\hat{p}_i \cdot \hat{k}_r\right)^2\right] \tag{21}$$

$$F_{\mathrm{D}} = \frac{\pi^2 L_c^2}{4\lambda_L^2} \sum_{m=1}^{\infty} \frac{F_r^m \exp(-F_r)}{m \cdot m!} \exp\left[-\frac{\left(k_{\mathrm{dx}}^2 + k_{\mathrm{dy}}^2\right) L_c^2}{4m} \right] \quad (22)$$

Here, $\hat{k}_m$ $\hat{P}_m$ and $\hat{s}_m$ are the unit vectors along the direction of the laser beam propagation and the *p*- and *s*-polarizations, respectively, with the subscript $m = i$ and r for the incident and reflected beams, respectively. $\vec{k}_d$ is the change in the wave vector due to the reflection, which is given by $\vec{k}_d = \hat{k}_r - \hat{k}_i = k_{\mathrm{dx}}\hat{x} + k_{\mathrm{dy}}\hat{y} + k_{\mathrm{dz}}\hat{z}$, where $\hat{x}$, $\hat{y}$ and $\hat{z}$ are the unit vectors along the x, y and z axes in Cartesian coordinates, and k_{dx}, k_{dy} and k_{dz} are the x-, y- and z-components of the vector $\vec{k}_{\mathrm{d}}$, respectively.

Integrating $\bar{R}_b(\theta_r)$ over the acceptance angle, $\Delta\theta_a$, of the photodetector, i.e., from $\theta_{\mathrm{rs}} - \frac{1}{2}\Delta\theta_a$ to $\theta_{\mathrm{rs}} + \frac{1}{2}\Delta\theta_a$, the total reflectance around the specular direction for rough surfaces ($\bar{R}_{\mathrm{sr}}$) is obtained from the following expression where θ_i is used in the limits of integration since the specular reflection angle $\theta_{rs} = \theta_i$:

$$\bar{R}_{\mathrm{sr}} = \int_{\theta_i - \frac{1}{2}\Delta\theta_a}^{\theta_i + \frac{1}{2}\Delta\theta_a} \bar{R}_b(\theta_r, \rho_{\mathrm{rms}}) \mathrm{d}\theta_r \quad (23)$$

Similarly the total reflectance around the specular reflection direction for a smooth surface ($\bar{R}_{\mathrm{ss}}$) can be obtained from Eq. (23) by considering a very small value of the surface roughness that is taken as $\rho_{\mathrm{rms}} = 0.1$ nm in this study. A photodetector of diameter 25.4 mm was used in this study to measure the reflected power of a laser beam of wavelength 1,064 nm in the specular reflection direction for various samples in order to calculate the experimental reflectance. This dimension of the detector and its placement from the sample resulted in $\Delta\theta_a = 33.7°$ for the theoretical reflectance. For the case of smooth surface, the Fresnel reflectivity is obtained from Eqs. (12) and (13), and then, the reflectance of the rough surfaces are calculated using the following expression:

$$R_{\mathrm{th}} = \frac{\bar{R}_{\mathrm{sr}}}{\bar{R}_{\mathrm{ss}}} R_F \quad (24)$$

The values of ρ_{rms} for different samples and the corresponding results for $\bar{R}_{\mathrm{sr}}$, $\bar{R}_{\mathrm{ss}}$, R_F and R_{th} are listed in Tables 1 and 2.

3 Laser diffusion experiment

Accessories for typical laser diffusion experiments include a laser to heat up the substrate in which diffusion occurs, a precursor for the diffusant atoms and a vacuum chamber in which the precursor is heated at the laser–substrate interaction zone. The diffusant atoms are produced due to thermochemical decomposition of the precursor and, subsequently, they diffuse into the substrate.

Table 1 Surface properties and reflectivities of Ti and Ta samples

Sample (μm)	ρ_{rms} (μm)	ρ_{fit} (μm)	$\bar{R}_{\mathrm{sr}}$	$\bar{R}_{\mathrm{ss}}$	R_{F} (%)	R_{th} (%)
Ti 25	0.205	0.025	34.91	37.44	56.0	52.37
Ti 50	0.235	0.04	32.82	37.44	56.0	49.23
Ta 25	0.4	0.4	28.24	60.11	89.9	42.36
Ta 50 (As-received)	0.8	0.8	21.99	60.11	89.9	33.0
Ta 50 (Roughened)	0.847	0.847	17.89	60.11	89.9	26.84

Table 2 Surface properties of Ti and Ta samples

Sample (μm)	ρ_{rms} (μm)	ρ_{fit} (μm)	$\bar{R}_{\mathrm{sr}}$	$\bar{R}_{\mathrm{ss}}$	R_{F} (%)	R_{th} (%)
(a) linear polarization						
Ti 25	0.205	0.025	28.4	29.52	44.2	42.60
Ti 50	0.235	0.04	26.95	29.52	44.2	40.40
Ta 25	0.4	0.4	30.02	57.54	86.1	45.0
Ta 50 (As-received)	0.8	0.8	28.91	57.54	86.1	43.37
Ta 50 (Roughened)	0.847	0.847	23.13	57.54	86.1	34.70
(b) Azimuthal polarization						
Ti 25	0.205	0.025	34.70	36.97	55.3	52.04
Ti 50	0.235	0.04	32.87	36.97	55.3	49.31
Ta 25	0.4	0.4	31.18	59.78	89.4	46.77
Ta 50 (As-received)	0.8	0.8	30.01	59.78	89.4	45.02
Ta 50 (Roughened)	0.847	0.847	24.02	59.78	89.4	36.03

3.1 Precursor selection

Usually the precursors are organometallic compounds containing the diffusant atoms. Thurier and Doppelt [24] investigated different Pt precursors, including $Pt(acac)_2$ (acac = $C_5H_7O_2$), $Pt(PF_3)_4$, $Pt(CO)_2Cl_2$, $PtMe_2(MeCN)_2$, $CpPtMe_3$ (Me = CH_3, Cp = cyclopentadienyl), MeCpPtMe$_3$, (acac)PtMe$_3$, (cod)PtMe$_2$ (cod = 1,5-CycloOctaDiene), CpPtMe(CO), (cod)(Cp)PtMe, (cod)PtMeCl and CpPt(allyl) for chemical vapor deposition application and reported the effect of different reactive species such as hydrogen, oxygen and water vapor on the deposition of Pt on various substrates. Many of these Pt precursors, however, are not readily available commercially. Platinum(II) acetylacetonate [$Pt(C_5H_7O_2)_2$ or $Pt(acac)_2$] is chosen in this study because it is readily available, insensitive to air and moisture, and less toxic than other commercially available Pt precursors. Also $Pt(acac)_2$ vaporizes at a low temperature (180 °C at 20–200 μTorr [24]), and its thermochemical decomposition begins to occur at a relatively low

temperature of 210–240 °C [25] compared to the other Pt precursors. The products of this chemical reaction are [26]:

$$\mathrm{Pt(acac)2} \rightarrow \mathrm{Pt} + \mathrm{CH3COCH2COCH3}.$$

3.2 Diffusion experiment

Ti and Ta sheets were used as the substrates in this study. Each sample was a square sheet of side 20 mm and thickness 25 or 50 μm. The substrates were prepared by cleaning the sheets in acetone and deionized water ultrasonic bath. Diffusion experiments were conducted by placing each substrate in a laser diffusion chamber as illustrated in Fig. 4. The edges of the Ti or Ta sheets were placed between two copper frames that were held together with screws. The top surface of the sheet was exposed to the incident laser beam, while the bottom surface was exposed to the environment inside the vacuum chamber. This sample holder enables convection cooling at both the bottom and top surfaces, and prevents distortion of the sheets due to thermal stresses. 0.2 g of the Pt precursor ($Pt(acac)_2$) was dissolved in 20 cm^3 of acetylacetone [$CH_3COCH_2COCH_3$], and the solution was heated in a bubbler using a hot plate maintained at 130 °C to generate sufficient vapor pressure [25]. The pressure inside the diffusion chamber was lowered to 5 mTorr, and then, argon gas was passed through the bubbler to transport the precursor vapor to the chamber to achieve a pressure of 2 atm. A Nd:YAG laser of wavelength 1,064 nm was used to heat the substrate, resulting in thermochemical decomposition of the Pt precursor at the laser-heated spot. The Pt atoms that are produced due to this chemical reaction diffuse into the substrate. Acetylacetone, the other product of the thermochemical reaction, might decompose into acetone, carbon monoxide, carbon dioxide and methane at different temperatures. All the products except Pt are gaseous or evaporate easily at room temperature.

The laser processing parameters, such as the laser power, beam diameter and scanning speed, were selected to achieve sufficiently high temperatures for the formation and diffusion of Pt atoms without melting the substrate. The direction of the electric field in the laser beam was varied as random, linear, circular and azimuthal polarization to study its effect on the diffusion of Pt. We have examined two sets of samples for each of Ti and Ta sheets, which are as-received and laser-platinized samples. Beam shaping lens and polarizers were used as shown in Fig. 5 to generate polarized flat-top laser beams. Since the laser system, which was used in this study, produces a randomly polarized laser beam, only a beam shaping lens is used to generate a randomly polarized flat-top laser beam. A linear polarizer and a beam shaping lens generate a linearly polarized flat-top laser beam. Using a linear polarizer, quarter wave plate and a beam shaping lens, a circularly polarized flat-top beam is produced. A linear polarizer, a phase plate [27] and a beam shaping lens were used to produce an azimuthally polarized flat-top beam.

For the Ti sheets, two laser scanning speeds $u = 6$ and 12 mm/s were chosen for the laser power 12 W, and two polarizations were tested. Due to the thermophysical properties of Ta, more laser energy is necessary to heat the Ta substrates for diffusing Pt into Ta than in the case of Ti substrates. The Ta sheets were, therefore, treated with higher laser power (16 W) and lower scanning speeds ($u = 3$ and 6 mm/s) than in the case of Ti sheets. Even with these processing parameters, the 50-μm-thick Ta sheets were not sufficiently heated to induce the thermochemical reaction for the formation of Pt atoms. These thick Ta sheets were roughened with sandpaper (grade 2000) to increase the absorption of laser energy at the rough surface.

The laser diffusion experiments were carried out by placing each substrate 21 mm below the beam shaping lens (BSL in Fig. 5) inside the vacuum chamber. A beam expander consisting of a plano-concave lens and a plano-convex lens of focal lengths −30 and 40 mm, respectively, was used to expand the output beam of the laser system from a radius of 0.75–0.8 mm. The radius of the flat-top laser beam was 1 mm on the substrate surface. The irradiance profile of the laser beam on the substrate surface was measured using a CCD camera-based profilometer, showing a fairly uniform energy distribution across the laser beam as presented in Fig. 6. Many passes of the laser beam were used to diffuse Pt over a large surface of the substrate.

4 Results and discussion

The laser heating of metals largely depends on their reflectivity among other parameters such as the laser irradiance and scanning speed. Therefore, the optical quality of the substrate surface was characterized by reflectivity, which was measured at two angles of incidence, $\theta_i = 0$ and 45°, as shown in Fig. 7. The reflectivity was also calculated using the above-mentioned rough surface reflection model. The measured reflectivities are compared to the theoretical values in Fig. 7 for random (R), p (L_p—linear polarization), circular (Cir) and azimuthal (Az) polarizations, respectively. The Fresnel reflectivity for random, circular and azimuthal polarizations is taken as $\left(R_{\mathrm{Fp}} + R_{\mathrm{Fs}}\right)/2$. The complex refractive indices of Ti and Ta at the wavelength of 1,064 nm are $3.47 + i3.4$ and $0.93 + i5.75$, respectively [28]. The substrate surface roughness data are listed in Tables 1 and 2. The reflectivities of Ti samples are close to the Fresnel reflectivities because the surface roughnesses of

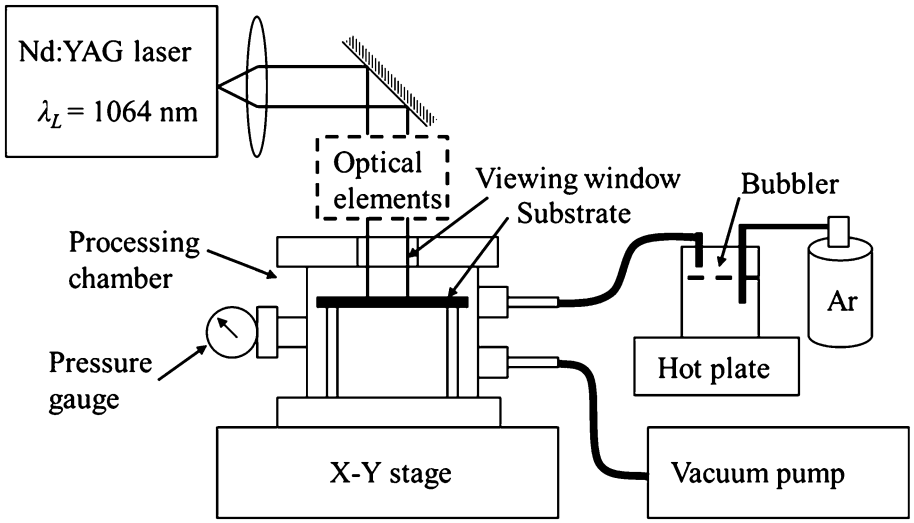

Fig. 4 A typical laser diffusion system to incorporate diffusant atoms into substrates

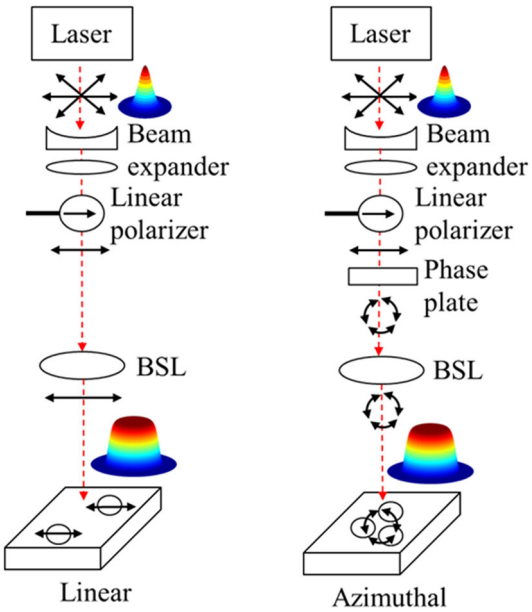

Fig. 5 Optical elements used to generate polarized flat-top laser beams

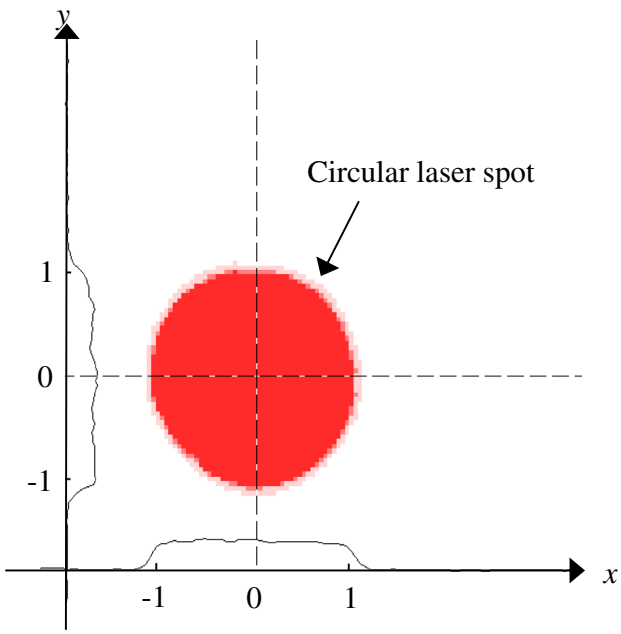

Fig. 6 Irradiance profile of the flat-top laser beam

Ti samples are much smaller than the laser wavelength of 1,064 nm. Therefore, the Ti samples can be considered to have smooth surfaces for which the Fresnel reflection formulae are applicable. The reflectivity of Ta samples, on the other hand, is less than half of the Fresnel reflectivity due to large surface roughness that is comparable to the laser wavelength. The reflectivities of the Ta samples are higher at the incident angle of 45° than at normal incidence due to smaller effective surface roughness at oblique incidence. This phenomenon is not significant for Ti samples due to smoother surface. At the normal incidence, the reflectivities of the samples are the same for all polarizations because the electric field of laser beam oscillates the atoms on the surface plane of the samples. At oblique incidence, the reflectivity of *p*-polarized laser beams is lower than that of randomly, circularly, azimuthally and *s*-polarized laser beams because the amplitude vector of *p*-polarized laser beams is not parallel to the surface plane of samples and, therefore, cannot oscillate the atoms as much as other polarizations.

The values of theoretical surface roughness (ρ_{fit}), which are listed in Tables 1 and 2 and used in the above-mentioned rough surface reflection model, are selected to achieve the best fits between the experimental and

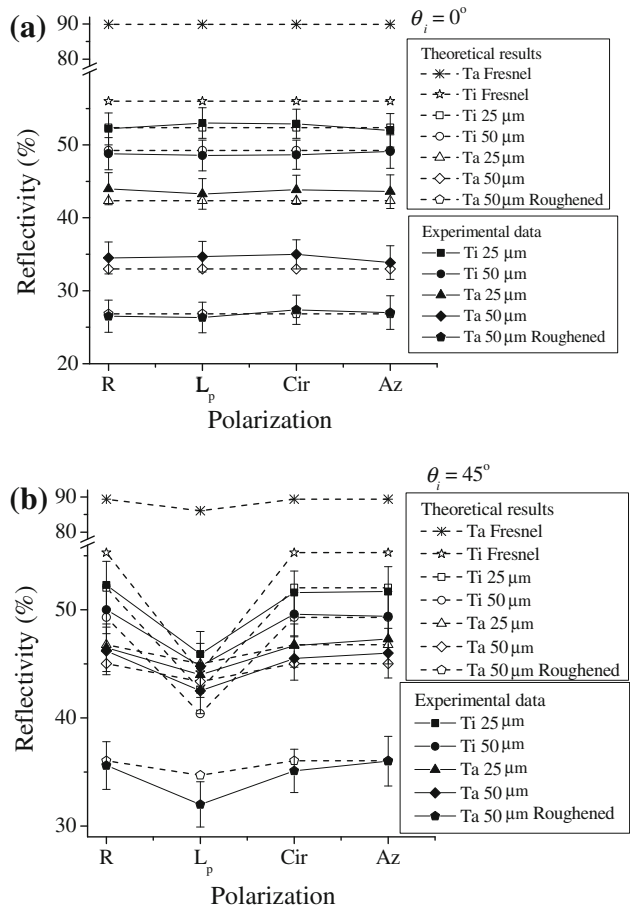

Fig. 7 Experimental and theoretical reflectivities of as-received samples for random (R), p (L_p), circular (Cir) and azimuthal (Az) polarizations: **a** normal (0°) incidence and **b** oblique (45°) incidence

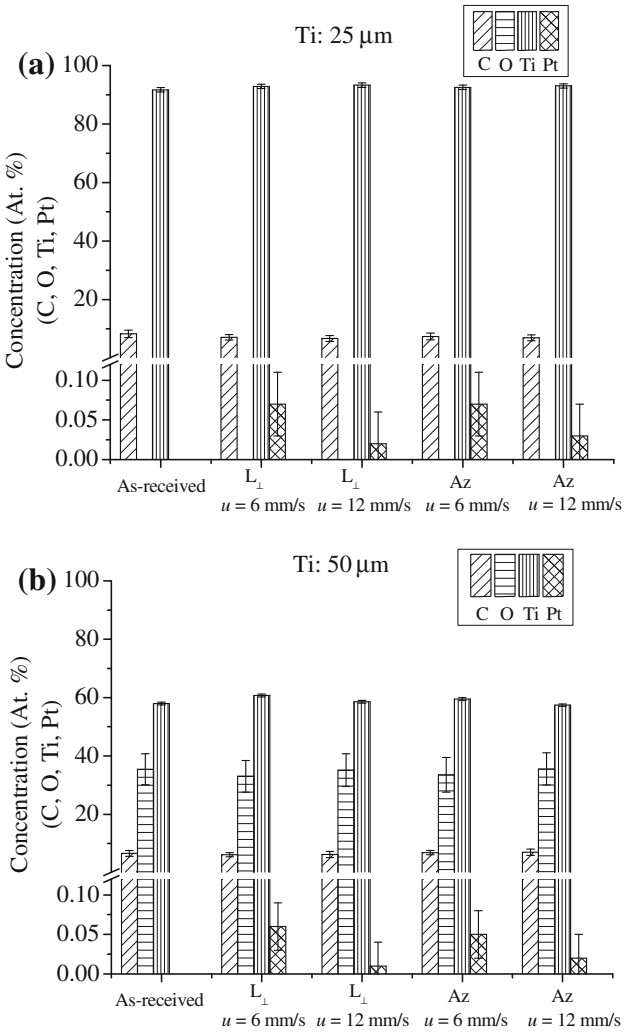

Fig. 8 Concentrations of different elements in laser-treated, **a** 25-μm-thick and **b** 50-μm-thick Ti samples

theoretical reflectivities for the Ti and Ta samples as presented in Fig. 7. The value of the acceptance angle of the photodetector was 33.7° in this study. The theoretical surface roughnesses of Ti samples are different from the experimental data for two possible reasons. The surface of Ti samples can be considered smooth due to their small roughness, and the model is based on the approximation that either the surface is very rough i.e., $(2\pi\rho_{\mathrm{rms}}/\lambda)^2 \gg 1$, or the surface slope is gentle i.e., $\rho_{\mathrm{rms}}/L_c \ll 1$ [29].

The concentrations of impurities in the Ti and Ta samples were determined by energy-dispersive x-ray spectroscopy (EDS). After the laser diffusion experiments, all of the samples were cleaned in acetone and deionized water ultrasonic bath before the EDS measurement. The electron beam penetrates a certain distance into the substrate during EDS, resulting in a spatial resolution over a certain cross-sectional area depending on the beam diameter and a certain depth depending on the penetration depth. This yields a volumetric resolution, which is approximately a sphere of diameter 1 μm, for the measurement. Since the maximum concentration occurs at the surface, the surface analysis technique is used in this study, and the EDS data represent the concentration over the volumetric resolution. The concentrations of impurities in the Ti samples are plotted in Fig. 8a, b for two thicknesses, two scanning speeds, and for azimuthal (Az) and linear (L⊥) polarizations, where L⊥ represents the polarization direction perpendicular to the scanning direction of the laser beam. The as-received 25-μm-thick Ti sample contains carbon (C) impurity, and the as-received 50-μm-thick Ti sample contains C and oxygen (O) impurities. The colors of these two samples were different with silver and yellowish appearances for 25- and 50-μm-thick Ti samples, respectively, which might be attributed to the difference in chemical compositions. After the laser diffusion experiments, the presence of Pt atoms is observed in the laser-treated samples, and the concentrations of C and O do not change significantly (Fig. 8). The concentration of Pt atoms is higher at the

lower scanning speed due to higher surface temperature and longer laser–substrate interaction time providing longer time for the diffusion of Pt atoms into the substrate.

The substrate surface temperature due to laser irradiation can be estimated by the expression: $T_s = T_i + \frac{P_L(1-R)\tau}{2r_0 u\tau d\rho C_p + 2r_0 u\tau^2 h_b + 2u\tau^2 dh_l}$, where T_s is the surface temperature, T_i is the initial temperature of the substrate, P_L is the incident laser power, R is the reflectivity of the substrate at the laser wavelength, which is measured for different polarizations and surfaces roughnesses in this study, and τ is the laser–substrate interaction time given by $2r_0/u$ for a laser beam of radius r_0 and laser scanning speed u. d, ρ and C_p are the thickness, density and specific heat capacity of the substrates, respectively, h_b is the heat transfer coefficients at the bottom and top surfaces of the substrate and h_l is the lateral heat transfer coefficient of the substrate. Although the free convection heat transfer coefficient is typically low (2–25 W/m^2 K) for gases, h_b is chosen as 200 W/m^2 K in this study to account for high (2 atm) gas pressure inside the chamber and the loss of thermal energy from the substrate to heat up the reactant molecules. h_l is estimated as the ratio of thermal conductivity (k_{th}) of the substrate to the laser beam radius (r_0), which yields $h_l = 2.2 \times 10^4$ and 5.8×10^4 W/m^2 K for Ti and Ta substrates, respectively. The density (ρ), specific heat capacity (C_p) and thermal conductivity (k_{th}) of Ti and Ta are 4,500 kg/m^3, 522 J/kg K and 21.9 W/m K, and 16,600 kg/m^3, 140 J/kg K and 57.5 W/m K, respectively.

Based on these data, the calculated surface temperatures are plotted in Fig. 9, showing higher surface temperatures at lower scanning speeds. Since the diffusion coefficient generally increases as the temperature increases, higher Pt concentration is observed in the Ti samples that are laser-treated at the scanning speed of 3 mm/s. It should be noted that the reflectivity, R, affects the surface temperature significantly. Since many passes of the laser beam were used to produce a large modified surface, the reflectivity of the overlapped laser tracks on the substrate surface can be different from the single track regions during the laser doping process. However, the amount of Pt that is diffused into the substrate is very small and, therefore, the reflectivity is not expected to vary significantly in these two types of tracks. So the measured reflectivity of the as-received samples can be utilized to determine the temperature of the laser-heated spot during the diffusion process. Although pyrometry, which is a nonintrusive technique, can be employed to remotely measure the temperature beneath the laser beam, the accuracy of the measurement depends significantly on the emissivity of the surface. Due to the lack of emissivity data at high temperatures, the surface temperatures are estimated to analyze the trend in the concentration of diffused Pt.

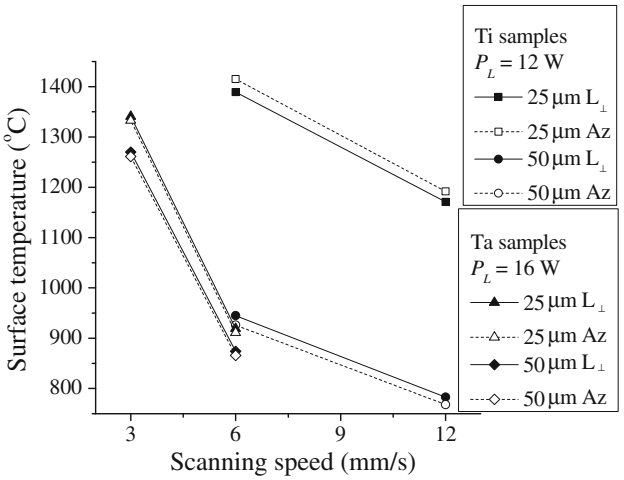

Fig. 9 Theoretical surface temperatures of samples irradiated with Nd:YAG lasers of linear and azimuthal polarizations

The concentrations of impurities in the Ta samples are plotted in Fig. 10a, b for two thicknesses, two scanning speeds and two polarizations of the laser. The as-received Ta substrates contain C and O impurities. The laser-treated Ta samples are found to contain Pt atoms with higher concentration at the lower scanning speed. Higher surface temperatures at lower scanning speeds enable increasing the Pt concentration as in the case of Ti samples. However, the Pt concentration in 50-μm-thick Ta samples, which were laser-treated at the scanning speed of 6 mm/s, is below the detection limit of the EDS system because the surface temperature was not sufficiently high to provide a thermal condition for the formation of Pt atoms and their diffusion into the substrate. The concentration of O is found to increase in the laser-treated Ta samples compared to the as-received samples.

The Ta samples that were irradiated with linearly polarized laser beams have slightly higher Pt concentration than those irradiated with azimuthally polarized laser beams. Since the reflectivity of the substrate is slightly lower for linear polarization than for azimuthal polarization, the substrate surface temperature is correspondingly slightly higher for the linearly polarized laser beams. Therefore, enhancement in the thermochemical reaction for the production of Pt atoms and increase in the diffusion coefficient at higher temperatures may be attributed to the observed higher Pt concentration in the samples treated with the linearly polarized laser beam. The linearly polarized laser beam can also excite the local vibration modes of the Pt and substrate atoms differently compared to the azimuthally polarized beam, resulting in higher Pt concentration in the substrate.

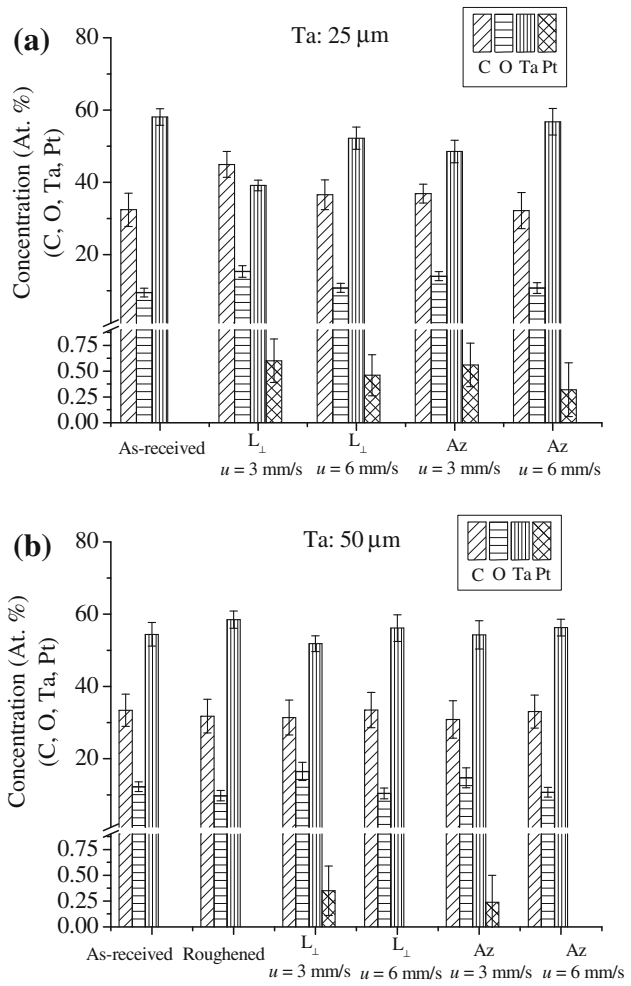

Fig. 10 Concentrations of different elements in laser-treated, **a** 25-μm-thick and **b** 50-μm-thick Ta samples

5 Conclusions

Thin sheets of Ti and Ta have been heated with laser beams of different polarizations to diffuse Pt into the sheets without melting the sheets. The reflectivities of the sheets are measured for four polarizations of a Nd:YAG laser and compared with theoretical results. When the surface roughness is small compared to the laser wavelength, the surface can be considered smooth for which the measured reflectivity is almost equal to the Fresnel reflectivity. On the other hand, when the surface roughness is comparable to the laser wavelength, the effects of surface asperity dominate and the reflectivity is significantly lower than the Fresnel reflectivity. The reflectivities are almost the same for the four polarizations at normal incidence, while the reflectivity for *p*-polarization is lower than the other three polarizations at the incident angle of 45°. For the same polarization, however, the reflectivity at oblique incidence is higher than at the normal incidence due to the smaller effective roughness of the surface.

Based on the measured reflectivity of the Ti and Ta sheets, the substrate surface temperature is estimated during laser irradiation to analyze the Pt content in the laser-treated samples. The concentrations of C and O impurities and laser-diffused Pt atoms in the Ti and Ta samples are measured using EDS. Higher concentrations of Pt atoms are observed in the samples that are laser-treated at lower scanning speeds. This result may be due to higher surface temperatures produced at lower scanning speeds for the same irradiance of the laser beam. Slightly higher Pt concentration is obtained with linear polarization than with azimuthal polarization, because of lower reflectivity and, consequently, higher surface temperature in the former case. Also the linearly polarized laser beams may facilitate the migration of Pt atoms in the substrate by affecting the phonons differently compared to the azimuthally polarized laser beams.

References

1. S. Bet, N.R. Quick, A. Kar, Laser doping of chromium in 6H-SiC for white light-emitting diodes. J. Laser Appl. **20**, 43–49 (2008)
2. G. Lim, U.P. DeSilva, N.R. Quick, A. Kar, Laser optical gas sensor by photoexcitation effect on refractive index. Appl. Opt. **49**, 1563–1573 (2010)
3. K.H. Weiner, T.W. Sigmon, Thin-base bipolar transistor fabrication using gas immersion laser doping. IEEE Electr. Device Lett. **10**, 260–263 (1989)
4. D. Petring, P. Abels and E. Beyer, Absorption distribution on idealized cutting front geometries and its significance for laser beam cutting, Proc. SPIE, High Power CO2 Laser Systems and Applications, Vol. 1020, edited by A. Quenzer, (SPIE, Bellingham, 1988), pp 123–131
5. V.G. Niziev, A.V. Nesterov, Influence of beam polarization on laser cutting efficiency. J. Phys. D Appl. Phys. **32**, 1455–1461 (1999)
6. C.-Y. Ho, Effects of polarizations of a laser on absorption in a paraboloid of revolution-shaped welding or drilling cavity. J. Appl. Phys. **96**, 5393–5401 (2004)
7. M. V. Artsimovich, A. N. Baranov, V. V. Krivov, Eugene M. Kudriavtsev, Emma N. Lotkova, B. H. Makeev, I. F. Mogilnik, V. N. Pavlovich, B. N. Romanuk, V. I. Soroka, V. V. Tokarevski and Sergey D. Zotov, Resonant IR laser-induced diffusion of oxygen in silicon, Proc. Eighth Intl. Symp. On Gas Flow and Chemical Lasers (SPIE 1397), (SPIE, Madrid, 1991), pp. 729-733
8. V.N. Pavlovich, Influence of radiation polarization on laser-enhanced resonance diffusion in crystals. Sov. Phys. Solid State **32**, 1315–1317 (1990)
9. Y. Belvaux, S.P.S. Virdi, A method for obtaining a uniform non-Gaussian laser illumination. Opt. Commun. **15**, 193–195 (1975)
10. Y. Ozaki, K. Takamoto, Cylindrical fly's eye lens for intensity redistribution of an excimer laser beam. Appl. Opt. **28**, 106–110 (1989)
11. C.H. Chen, C.C. Chen, W.C. Liang, Light pine line beam shaper. Opt. Rev. **14**, 231–235 (2007)
12. D.R. Brown, Laser beam shaping with diffractive diffusers, in *Laser beam shaping*, ed. by F.M. Dickey (Marcel Dekker, New York, 2000), pp. 249–271
13. Z. Tian, N.R. Quick, A. Kar, Laser-enhanced diffusion of nitrogen and aluminum dopants in silicon carbide. Acta Materiallia **54**, 4273–4283 (2006)

14. S. Bet, N.R. Quick, A. Kar, Effect of laser field and thermal stress on diffusion in laser doping of SiC. Acta Materiallia **55**, 6816–6824 (2007)
15. G. Manivasagam, D. Dhinasekaran, A. Rajamanickam, Biomedical implants: corrosion and its prevention—a review. Recent Pat. Corros. Sci. **2**, 40–54 (2010)
16. A. Cowley, B. Woodward, A healthy future: platinum in medical applications. Platin. Met. Rev. **55**, 98–107 (2011)
17. J.D. Jackson, *Classical Electrodynamics* (Wiley, New York, 1999), p. 487
18. G.D. Gillen, C.M. Seck, S. Guha, Analytical beam propagation model for clipped focused-Gaussian beams using vector diffraction theory. Opt. Express **18**, 4023–4040 (2010)
19. M. Born, E. Wolf, *Principles of Optics* (Pergamon Press, New York, 1983), pp. 615–624
20. T.F. Smith, R.G. Hering, Bidirectional reflectance of randomly rough surface, in *Fundamentals of Spacecraft Thermal Design, Progress in Astronautics and Aeronautics*, vol. 29, ed. by J.W. Lucas (AIAA, New York, 1972), pp. 69–85
21. T.F. Smith, K.E. Nichols, Effects of polarization on bidirectional reflectance of a one-dimensional randomly rough surface, in *Spacecraft Radiative Transfer and Temperature Control*, vol. 83, ed. by T.E. Horton (AIAA, New York, 1981), pp. 3–21
22. R.L. Cook, K.E. Torrance, A reflectance model for computer graphics. ACM Trans. Graphics **1**, 7–24 (1982)
23. X.D. He, K.E. Torrance, F.X. Sillion, D.P. Greenberg, A comprehensive physical model for light reflection. Comput. Graphics **25**, 175–186 (1991)
24. C. Thurier, P. Doppelt, Platinum OMCVD processes and precursor chemistry. Coord. Chem. Rev. **252**, 155–169 (2008)
25. N.B. Morozova, G.I. Zharkova, P.P. Semyannikov, S.V. Sysoev, I.K. Igumenov, N.E. Fedotova, N.V. Gelfond, Vapor pressure of precursors for CVD on the base of platinum group metals. J. Phys. IV France **11**, 609–616 (2001)
26. J.V. Hoene, R.G. Charles, W.M. Hickam, Thermal decomposition of metal acetylacetonates: mass spectrometer studies. J. Phys. Chem. **62**, 1098–1101 (1958)
27. G. Machavariani, Y. Lumer, I. Moshe, A. Meir, S. Jackel, Efficient extracavity generation of radially and azimuthally polarized beams. Opt. Lett. **32**, 1468–1470 (2007)
28. D.R. Lide, *Handbook of Chemistry and Physics* (CRC Press, Boca Raton, 1991), pp. 12–112
29. A. Stogryn, Electromagnetic scattering from rough finitely conducting surfaces. Radio Sci. **2**, 415–428 (1967)